Available online at www.sciencedirect.com
SCIENCE DIRECT®
Journal of Power Sources 117 (2003) 273–282
JOURNAL OF POWER SOURCES
www.elsevier.com/locate/jpowsour

Electrochemical and capacitive properties of polyaniline-implanted porous carbon electrode for supercapacitors

Wei-Chih Chen, Ten-Chin Wen*

Department of Chemical Engineering, National Cheng Kung University, Tainan 701, Taiwan

Received 10 October 2002; accepted 27 January 2003

Abstract

Composite electrodes for supercapacitors were prepared by electropolymerization of polyaniline (PANI) on the surface of activated-porous carbons. The surface morphology and the chemical composition of composite electrodes were characterized by scanning electron microscopy (SEM) and X-ray photoelectron spectroscopy (XPS). The electrochemical properties of electrodes and the capacitive behavior of the resulting capacitors were systematically studied using cyclic voltammetry (CV), ac impedance and constant current charge–discharge tests. The specific capacitance of PANI-carbon composite electrode was exhibited as high as 160 F/g, in comparison with a value of 95 F/g for the bare-carbon (BC) electrode. An increase in capacitance more than 60% has been achieved, that identifies the significant contribution of pseudocapacitance from PANI on the overall capacitance.

Keywords: Supercapacitor; Polyaniline; Porous carbons; Pseudocapacitance

1. Introduction

Supercapacitors attract growing attention to the use of electrical energy storage systems because of higher specific power than batteries and higher specific energy than conventional capacitors, owing to the high capacitance of the electrode materials. According to the mechanisms of energy storage, two types of supercapacitor are under development. One is an electric double-layer capacitor (EDLC) in which energy storage is accumulated from the separation of electronic and ionic charges at the interface between a high surface area electrode and an electrolyte solution. The other one is a redox pseudo-capacitor, in which active species can be fast and reversibly oxidized or reduced at characteristic potentials.

In EDLCs, porous carbon is the most frequently used electrode material in recent years [1–5], due to the large surface area and porosity that ensure high specific capacitance. For pseudo-capacitors, metal oxide [6,7] and conjugated conducting polymers, such as polyaniline (PANI), polypyrrole, and polythiophene [8–10] have been investigated for use as electrode materials. Due to the existence of several different oxidation-state structures of these redox-active species over a potential range, high faradaic pseudocapacitance can be obtained.

Accordingly, an electrochemical capacitor when forms from an electrode material possessing large specific surface area and coupling with active species would exhibit both double-layer capacitance and faradaic pseudocapacitance simultaneously in energy storage. It is interesting to develop feasible composite electrodes of large specific capacitance made by incorporating PANI into porous carbons for the application of supercapacitors.

The purpose of this work is to enhance the capacitance of an EDLC via introduction of PANI to the activated carbon to fabricate composite electrodes. To prevent the carbon micropores from hindering by PANI particles, the amount of PANI has to be controlled adequately. The textural characteristics of the resulting electrodes are identified through scanning electron microscopy (SEM) and X-ray photoelectron spectroscopy (XPS). The electrochemical characteristics of electrodes and the practical performance of the constructed capacitors are also evaluated by using cyclic voltammetry (CV), ac impedance and charge–discharge experiments, to clarify the contribution of the PANI loading on the capacitance enhancement.

* Corresponding author. Tel.: +886-6-2385487; fax: +886-6-2344496.
E-mail address: tcwen@mail.ncku.edu.tw (T.-C. Wen).

0378-7753/03/$ – see front matter © 2003 Elsevier Science B.V. All rights reserved.
doi:10.1016/S0378-7753(03)00158-7

2. Experimental

2.1. Preparation of carbon electrodes

Porous carbon powders serving as the main electrode material (specific surface area 1778 m^2/g, pore volume 1.13 cm^3/g and average pore diameter 2.54 nm) were added to a solution of polyvinylidenefluoride (PVdF) in *N*-methyl pyrrolidinone (NMP), and the mixture was stirred at ambient temperature to form a carbon slurry. Carbon electrodes were fabricated by coating the slurry on stainless steel (type 304) foils, followed by evaporating the solvent, NMP, with a blow dryer. The carbon layer consisting of 20 wt.% PVdF as binder was controlled to have a thickness of 100 μm. This form of bare-carbon (BC) electrode is denoted as BC electrode.

2.2. Loading PANI on carbon electrodes

Reagent grade aniline (Merck) employed in the present work was doubly distilled and the resulting colorless liquid was kept under nitrogen in darkness at 5 °C.

Electrochemical polymerization of PANI was made by using the Autolab PGSTAT 30 (Eco. Chemie B.V., The Netherlands) with a general-purpose electrochemical system software. A three-electrode cell assembly was utilized with an Ag/AgCl reference electrode (Argenthal, 3 M KCl, 207 mV versus SHE at 25 °C). Platinum wire with a diameter of 0.5 mm and an exposed area of 0.65 cm^2 was used as the counter electrode. A bare-carbon electrode of area 1 cm^2 was used as the working electrode.

PANI particles were electrochemically loaded into the BC substrates through cyclic voltammetry (CV) by sweeping the potential in the range between −0.2 and 0.8 V. In order to avoid blocking the entrances of carbon micropores, the amount of PANI loading has to be a minimum. Hence, polymerization of aniline (ANI) using CV was conducted with a slow rate of 0.3 mV/s, and minimum cycles (three). Additionally, a low concentration (10 mM) of ANI in 1 M H_2SO_4 solution was used for the polymerization. Such PANI-implanted carbon electrode is denoted as PC electrode.

2.3. SEM

Micrographs of the electrodes (BC and PC) were obtained using a JXA-840 scanning electron microscope (JEOL, Japan). Photos were taken at vacuum after sputtering the sample with a thin gold film.

2.4. X-ray photoelectron spectroscopy

The chemical compositions were determined for the PC electrode by XPS using an ESCA 210 and MICROLAB 310D (VG Scientific Ltd., UK) spectrometer. Before scanning, the sample was sputtered by using Ar gas to remove absorbed impurities on the surface. For recording the spectra Mg Kα ($hv = 1253.6$ eV) irradiation was employed as the photon source with primary tension of 12 kV and an emission current of 20 mA. The pressure of the analysis chamber during the scans was about 10^{-10} mbar. Low-resolution survey scans were done at 50 eV pass energy by using a step of 1 eV to obtain the atomic percentage data. After the survey spectra were obtained, higher resolution survey scans were performed at pass energy of 20 eV, with a step of 200 meV, for at least 10 scans. Deconvolution of the XPS spectra was done by using Grams/32 software (Galactic).

2.5. Electrochemical measurements

Electrochemical measurements (CV and ac impedance) were carried out at ambient temperature using 1 M H_2SO_4 aqueous solution as electrolyte to examine the electrochemical performance of BC and PC electrodes. For the potential sweep cyclic voltammetric measurements, the potential scan rates were set as 0.5 and 1.0 mV/s within a potential range of −0.2 to 0.6 V. The cyclic voltammograms of the electrodes were recorded after stabilization.

The Impedance Spectrum Analyzer, IM6 (ZAHNER, Germany), with Thales software was employed to measure and analyze the ac impedance spectra of BC and PC electrodes obtained at different applied DC potentials. The potential amplitude of ac was kept as 10 mV and a wide frequency range of 50 mHz to 100 kHz was used.

Both the CV and electrochemical impedance spectroscopy (EIS) experiments were carried out in a three-compartment cell. BC or PC electrode was used as the working electrode. Platinum wire was used as the counter electrode. Ag/AgCl coupled with a Luggin capillary was used as the reference electrode.

2.6. Capacitance measurement

Sandwich-type capacitor cells were constructed with a pair of the electrodes, BC or PC, and a piece of filter paper as separator. The capacitance of the electrodes was galvanostatically measured with BT-2043 system (Arbin electrochemical instrument, USA), using 0.5 mA charge–discharge between 0 and 0.6 V for 1000 cycles.

3. Results and discussion

3.1. Textural characteristics of the resulting electrodes

PC electrodes were prepared by depositing PANI on BC electrodes by the method of cyclic voltammetry. To suppress the PANI loading on carbon, a low ANI concentration and a slow sweep rate were kept as 10 mM and 0.3 mV/s, respectively, only for three cycles during the polymerization.

Typical SEM photographs of the resulting BC and PC electrodes are shown in Fig. 1. In general, the surface

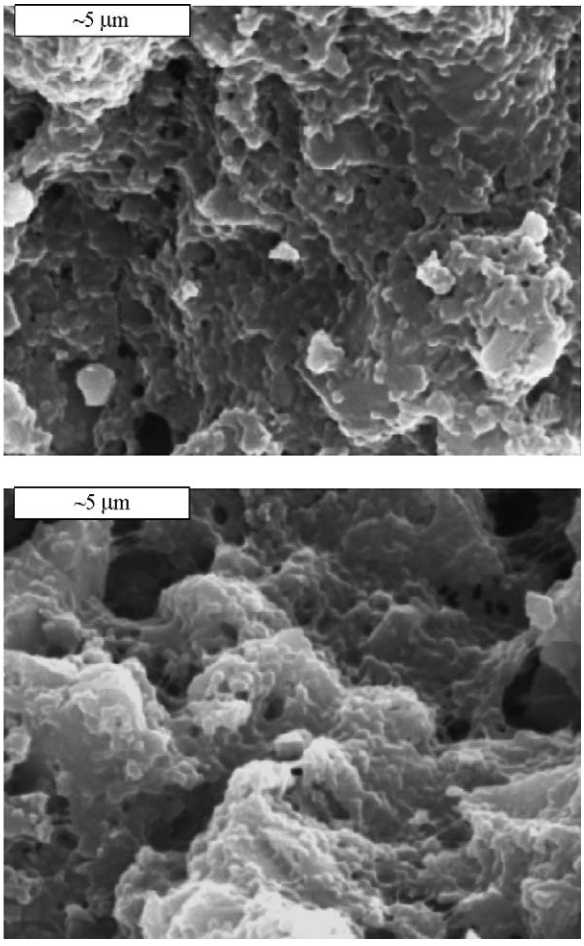

Fig. 1. SEM morphologies of (a) BC and (b) PC electrodes.

morphologies of both electrodes are rough and porous due to the intrinsic nature of activated carbon substrate. Note that, the morphology of carbon electrode is not significantly influenced by the deposition of PANI. When PANI was loaded on the substrate, the surface of PC electrode was partially covered by PANI particles, although no obvious difference in the morphology between these two electrodes was found (Fig. 1). This provides the evidence that the amount of PANI loading is controlled in minimum.

XPS scans were further taken to examine the surface composition of the PC electrode. Survey level XPS scan clearly reveals the presence of C, N, O, and S elements in the PC electrode. The relative atomic concentrations calculated from corresponding photoelectron peak area after sensitivity factor corrections (SF = 1.00, 1.77, 2.85 and 2.14 for C 1s, N 1s, O 1s and S 2p, respectively) are presented in Table 1. It can be obviously noticed from the data in Table 1 that the atomic percentage of N 1s of the PC electrode is 1.7%. The N element must come from the deposition of PANI on the electrode, since the complete absence of N signal on the pure carbon electrode has been previously reported [11].

The N 1s core level for the composite electrode can be deconvoluted into four components that are equal to the N 1s deconvolution of PANI film presented in earlier study [12]. These four species were assigned for C=N, C–N, $C=N^+$, and $C–N^+$ based on the binding energy of core electrons [12]. The N 1s spectrum is shown in Fig. 2, and the area ratio of the four components as well as their respective binding energy are given in Table 1. From the information in Table 1, the existence of S and O elements should result from the sulfate anions (SO_4^{2-}) which play the role as dopant attracted on the positive charge of the nitrogen atom. Otherwise, the carbons also trap the sulfate molecules in the micropores.

3.2. Electrochemical characteristics

Potential sweep cyclic voltammetric measurements were performed in a potential range between −0.2 and 0.6 V to examine the electrochemical characteristics of the resulting electrodes in 1 M H_2SO_4 solution. Figs. 3 and 4 show the voltammograms of the PC and BC electrodes, respectively, scanned with sweep rates of 0.5 and 1.0 mV/s. The voltammograms reveal both electrodes are stable in sulfuric acid solution within the sweeping potential range. Close comparisons of CV curves between PC and BC electrodes show that PC not only displays a higher background current in the potential sweep but also exists faradaic currents, which is expected to arise from the contribution of the loaded PANI. It has been reported that PANI was considered as promising materials for electrochemical capacitors due to the existence of different oxidation states [11,13,14]. Owing to the higher current in the voltammograms of the PC electrode than BC electrode, a larger capacitance for capacitors equipped with PC electrodes can be anticipated.

It is clear to see that the voltammograms present a little deviation from a rectangular form. A wide bending of voltammograms appears just after the reversal of the voltage sweep before reaching to the plateau. In the BC electrode, this phenomenon is resulted from the distributed capacitance

Table 1
Narrow scan XPS data for PC electrode

Electrodes	Atom (%)				N 1s[a]			
	C 1s	N 1s	O 1s	S 2p	C=N (399.3)[b]	C–N (400.4)	$C=N^+$ (401.3)	$C–N^+$ (402.5)
PC	64.1	1.7	28.8	5.4	18.1	33.6	28.8	19.5

[a] Area ratios of subpeaks.
[b] Binding energy of subpeaks, unit: eV.

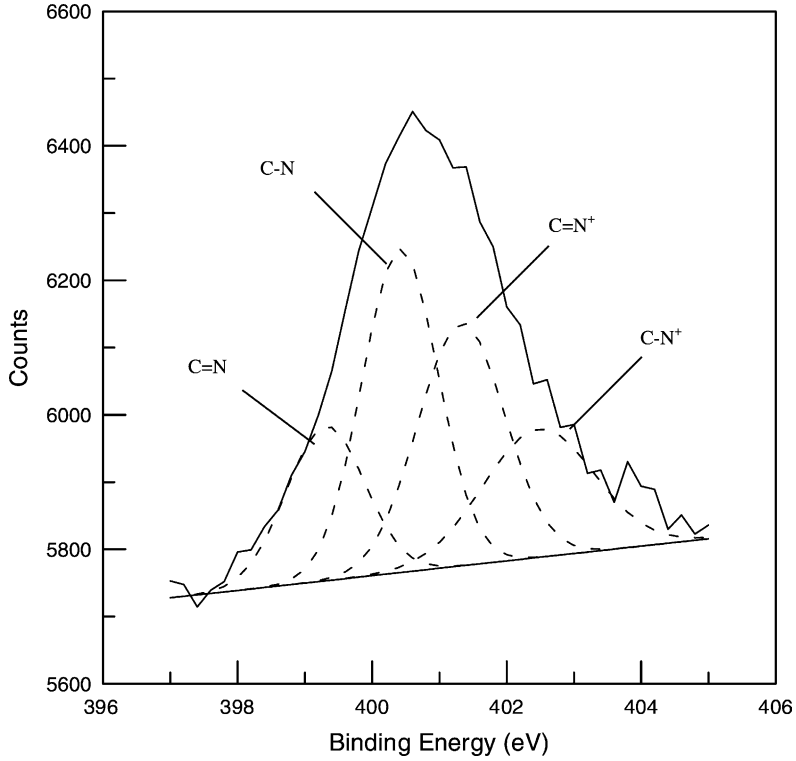

Fig. 2. XPS narrow scan of PANI-implanted carbon electrode for N 1s. The raw data (jagged curve) have been deconvoluted into Gaussian peaks.

effects in porous electrodes. Such effects were caused by the difference between the ohmic resistance of the electrolyte at the top of micropores and that at the bottom of micropores [5]. At the bottom, the resistance is serious for ion migration and influences the charge and discharge rates at the initial current inversion. Also, increasing the sweep rate aggravated the delay of the current to reach a horizontal value after reversal of the potential scan, which resulted from the fact that increasing the scan rate would lead to an increase in the potential difference and thus enhanced the lag of charge/discharge at the bottom of micropores.

However, the delay of current to reach to the plateau in the PC electrode is more significant than that in the BC electrode. This is due to the redox transitions of PANI were not as reversible and fast as the double-layer formation. Redox transitions of PANI also deform the voltammograms in shape of the PC electrode in comparison with the BC electrode. In Fig. 3, during the positive potential sweep,

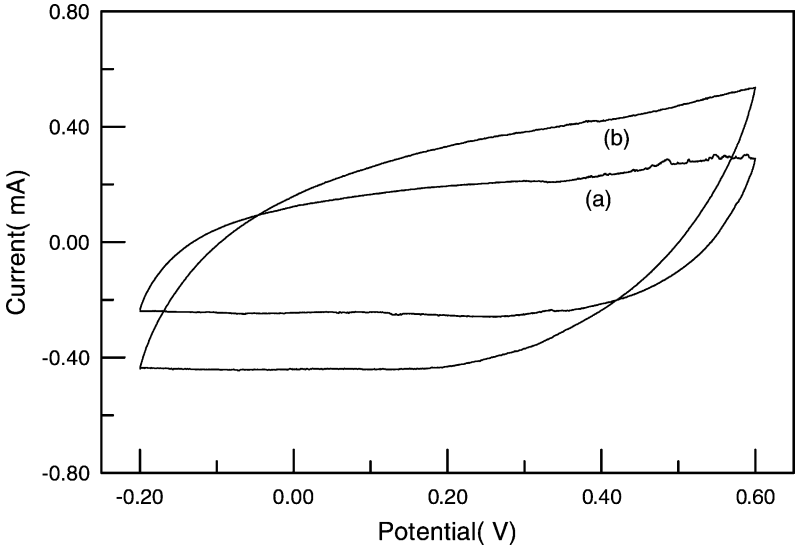

Fig. 3. Cyclic voltammograms of the PC electrode in 1 M H_2SO_4 at different sweep rates: (a) 0.5 and (b) 1.0 mV/s.

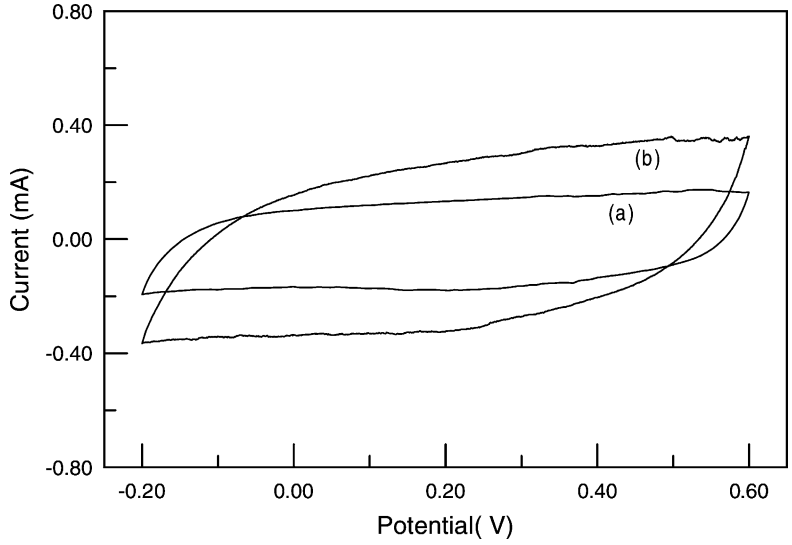

Fig. 4. Cyclic voltammograms of the BC electrode in 1 M H_2SO_4 at different sweep rates: (a) 0.5 and (b) 1.0 mV/s.

the current significantly increases with the potential beyond 0.2 V and progresses to a maximum at 0.6 V, which is attributable to the addition of faradaic current from PANI that is existing in the conducting emeraldine state. While PANI was in its insulated leucoemeraldine state (below 0.2 V), very low faradaic current was contributed. In the negative potential sweep, the enhanced current in the voltammograms was attributed to the reduction of PANI.

The further electrochemical information of the resulting electrodes was obtained by employing electrochemical impedance spectroscopy (EIS). The impedance spectra measured at different applied potentials for BC and PC electrodes are shown as Nyquist plots in Figs. 5 and 6, respectively. A single semi-circle in the high-frequency region and a straight line in the low-frequency region for all spectra can be observed. The high-frequency arc is the overall contact

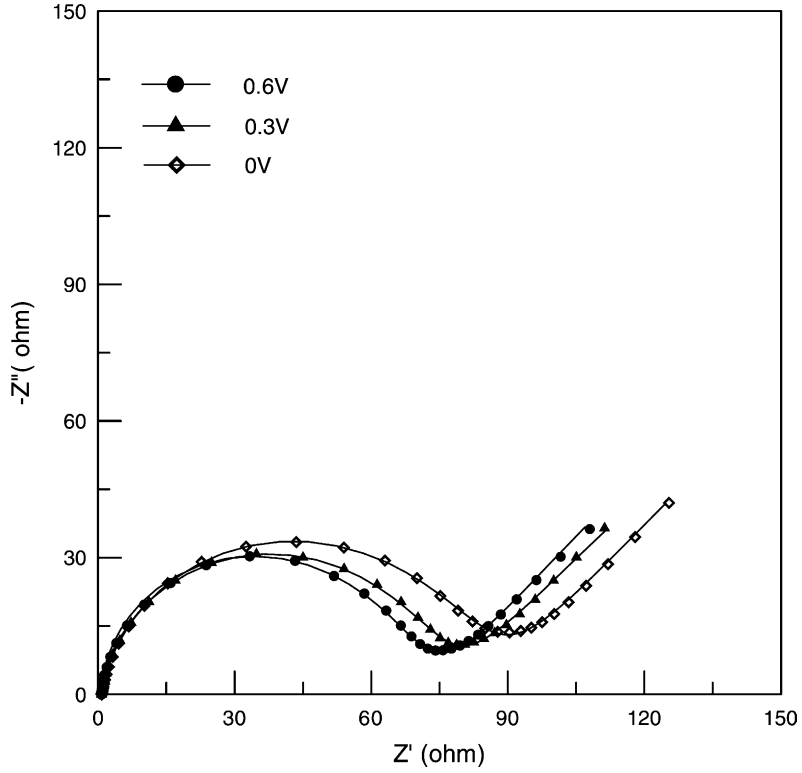

Fig. 5. Nyquist diagrams for the BC electrode measured at different applied potentials.

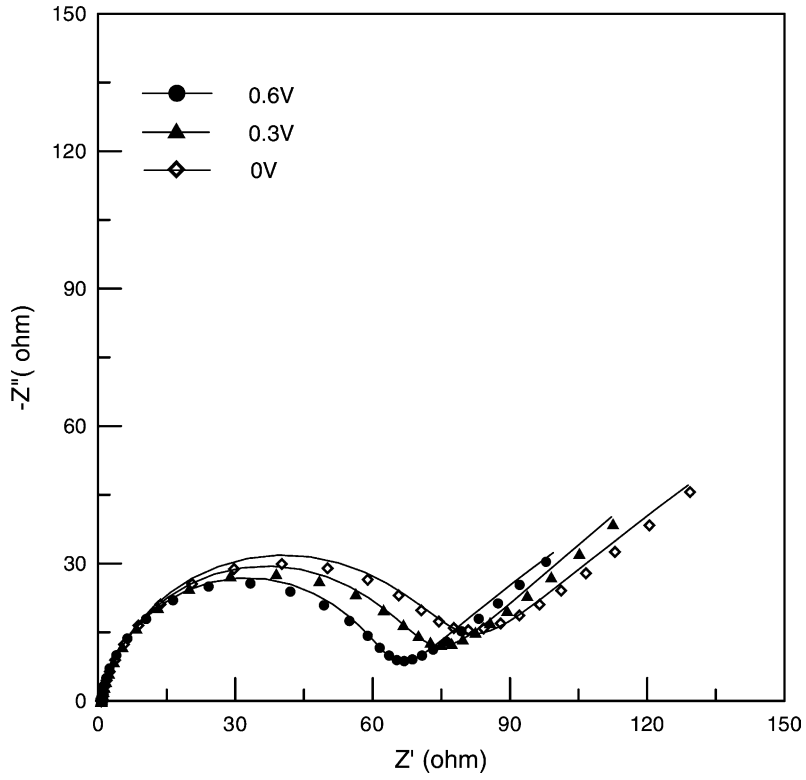

Fig. 6. Nyquist diagrams for the PC electrode measured at different applied potentials.

impedance generated from the electrical connection between carbon particles, and that between carbons and the backing plate as well as the charge transfer at the contact interface between the electrode and the electrolyte solution. Hence, the equivalent circuit for the electrodes was constructed by the following elements: the bulk solution resistance, R_S, the contact capacitance, C_C, which was expected in parallel with the contact resistance, R_C, and a Warburg diffusion element (Ⓦ) attributable to the diffusion of ions. Besides, the capacitive nature of the carbon-based electrode in the low-frequency domain could be reasonably presented as a low-frequency capacitance, C_L, in parallel with a charge transfer resistance, R_{ct}. Consequently, the circuit involving these elements is proposed in Fig. 7 to simulate the impedance spectra of both BC and PC electrodes [11]. For BC electrode, C_L expresses the double-layer capacitance (C_{dl}) attributable to the large surface area of activated carbons. However, in the case for PC electrode, C_L represents not only C_{dl} from carbon substrate but also the contribution of the pseudocapacitance (C_F) from PANI, which was attributable to the faradaic process of PANI redox transition. Regarding to the C_{dl} of carbons and C_F of PANI both appeared simultaneously in the low-frequency region [14,15], and therefore C_L was used alone to express the combination of C_{dl} and C_F for PC electrode. In addition, due to the porous surface of electrodes, a constant phase element (CPE) is used to express C_C and C_L in the equivalent circuit (Fig. 7) [16]. The CPE is defined in Eq. (1), where T, ω and α are the frequency-independent constants representing capacitance, angular frequency and a correction factor between 0 and 1, respectively. The physical meaning of this factor is related to the surface roughness of electrode surfaces.

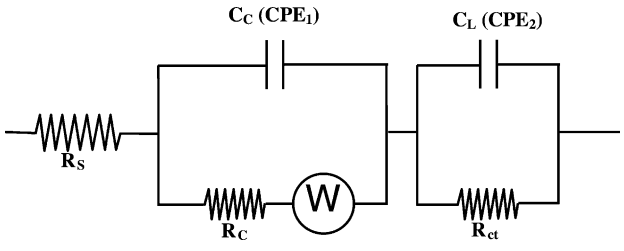

Fig. 7. Equivalent circuit for simulating the impedance spectra of the BC and PC electrodes. C_L represents C_{dl} and $C_{dl} + C_F$ for the BC and PC electrodes, respectively.

$$Z_{CPE} = T_{CPE}(j\omega)^{-\alpha}_{CPE} \quad (1)$$

The solid lines in Figs. 5 and 6 are the superimposed impedance data representing the best-fit curves based on the equivalent circuit in Fig. 7. The good fitting reveals that this equivalent circuit can successfully explain the electrochemical process occurring on/within BC and PC electrodes at different applied potentials. The best fitting values from EIS data for the electrochemical parameters corresponding to the circuit elements are listed in Table 2. The mean error of modulus is less than 0.6%, implying that the parameter values obtained from EIS fitting via such proposed circuit are highly reliable.

Table 2
The best fitting values of the equivalent circuit elements in Fig. 7 from the simulation of the impedance data for BC and PC electrodes at different applied potentials

Sample	Element	E (V)						
		0.0	0.1	0.2	0.3	0.4	0.5	0.6
BC electrode	R_S (Ω)	0.711	0.682	0.670	0.665	0.663	0.660	0.665
	R_C (Ω)	101.13	91.75	87.92	81.82	79.07	77.98	78.03
	CPE_1 (μF)	28.28	28.81	28.79	27.40	25.42	23.31	21.70
	α_1	0.938	0.946	0.956	0.963	0.972	0.988	0.971
	CPE_2 (F/g)	86.23	86.80	87.53	88.40	88.93	86.47	86.73
	α_2	0.958	0.956	0.945	0.964	0.946	0.958	0.962
PC electrode	R_S (Ω)	0.759	0.758	0.750	0.746	0.741	0.745	0.946
	R_C (Ω)	85.63	86.95	83.57	79.47	77.84	73.10	70.54
	CPE_1 (μF)	32.87	34.16	35.41	34.97	32.92	30.22	27.45
	α_1	0.873	0.864	0.882	0.883	0.898	0.901	0.912
	CPE_2 (F/g)	137.03	141.27	146.30	147.68	149.67	152.70	160.09
	α_2	0.958	0.969	0.986	0.972	0.989	0.958	0.981

Mean error of modulus is less than 0.6%.

CPE_2 (C_L) is the most concerned parameter in Table 2. Note that, CPE_2 for the BC electrode indicates the specific double-layer capacitance and achieves to about 88 F/g, which does not show apparent differences within the whole applied potential range. This result reveals that the double-layer structure in BC electrode would not be affected by the applied potentials. For the value of α_2, the correction factor of CPE_2, shows a slight deviation from 1. This suggests the double-layer element exhibiting as a non-ideal capacitor, due to the porous nature of the BC electrode unlike a flat plate. Hence, the limitation of ion migration in carbon micropores might cause a non-ideal capacitive behavior of the electrode.

The values of CPE_2 in the BC and PC electrodes are compared (Table 2). Obviously, a corresponding increase in CPE_2 of PC compared to BC is observed as well, which was owing to the coverage of PANI on the carbon surface. Also, the values of CPE_2 in the PC electrode appear to depend on the applied potentials. The value of CPE_2 varies from 137 to 160 F/g as the potential is applied between 0 and 0.6 V. This may be attributable to the implanted PANI that contributes the potential-dependent pseudocapacitance. At lower potentials, CPE_2 shows relatively small values, because of the insulated leucoemeraldine state of PANI. As the applied potential is raising, an obvious boost in CPE_2 value can be obtained. This phenomenon can be reasonably explained by the fact that PANI behaves as the electronically conductive emeraldine form at higher potentials and results in the occurrence of electrochemically reversible redox transitions. The trend of CPE_2 variation with the applied potential for the PC electrode (Table 2) is compatible with the current variation in the voltammograms shown in Fig. 3.

3.3. Charge–discharge cycling performance of capacitors

To illustrate the practical performance of the resulting PC electrodes in supercapacitors, constant current charge–discharge cycling was performed to measure the capacitance of the sandwich-type capacitor cells in 1 M H_2SO_4 solution. For the sake of making a close comparison, cells fabricated with the BC electrodes are also subjected to cycling tests. Typical galvanostatic charge–discharge curves at a current of 0.5 mA between 0 and 0.6 V are shown in Fig. 8. Obviously, it can be seen that the PC cell presents higher capacitance than the BC, which has been considered as the contribution of faradaic pseudocapacitance of PANI. Furthermore, to confirm the stability of the electrodes, the charge–discharge cycling test was continued to 1000 cycles. The specific discharge capacitance of the electrodes (C) in the cells was calculated from the following equation

$$C = \frac{2 \times I \times t}{W \times \Delta E} \quad (2)$$

where I is the discharge current, t the discharge time, W the material mass on an electrode, and ΔE the voltage difference in discharge, eliminating the section of IR drop. The factor of 2 comes from the fact that the total capacitance measured from the test cells is the addition of two equivalent single-electrode capacitors in series.

The variation of specific capacitance against cycle number for BC and PC electrodes are shown in Figs. 9 and 10, respectively. The results from Fig. 9 indicate the fact that BC capacitor has the capacitance about 95 F/g at the initial 50 cycles and keeps at 90 F/g in the 1000th cycle. This suggests BC electrodes remaining good stability over 1000 charge–discharge tests. As expectation, the specific capacitance of the PC capacitor is much higher than that of the BC, achieving 160 F/g at the early stage of cycling (Fig. 10). Consequently, the effect of implanting PANI on capacitance enhancement is significantly positive. The information observed from Fig. 10 illustrates the capacitance decayed from 160 to 144 F/g over 1000 cycles. This decay tells that

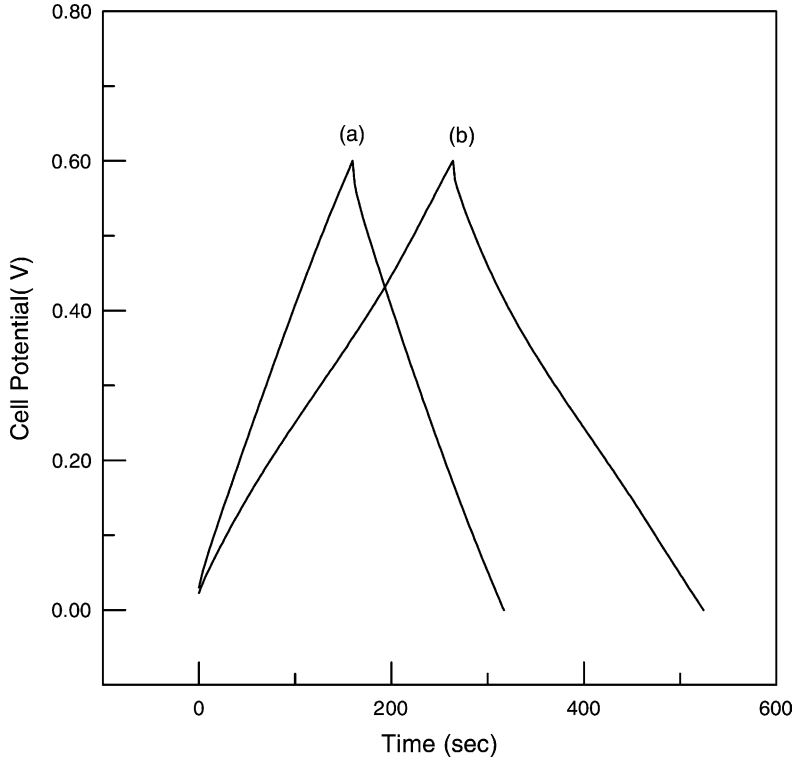

Fig. 8. Charge–discharge curves at 0.5 mA current of capacitors equipped with (a) BC and (b) PC electrodes.

the redox sites in the PANI backbone are insufficiently stable for many repeated redox processes, which is probably due to swelling and shrinking of PANI under aqueous environment and thus leads to the degradation of PANI during the long-term cycling [17]. Despite the decay of capacitance for the PC capacitor, an increase of more than 60% in capacitance compared to the BC is achieved. The exact values of specific capacitance obtained from charge–discharge cycling tests

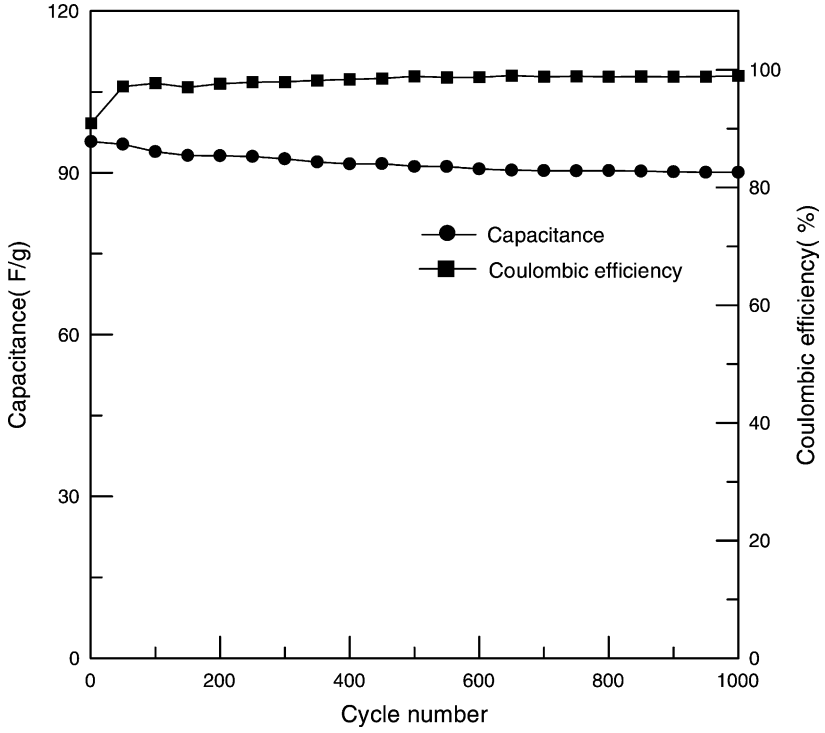

Fig. 9. Variation of capacitance and coulombic efficiency with cycle number for the BC electrode charged and discharged at 0.5 mA in 1 M H_2SO_4.

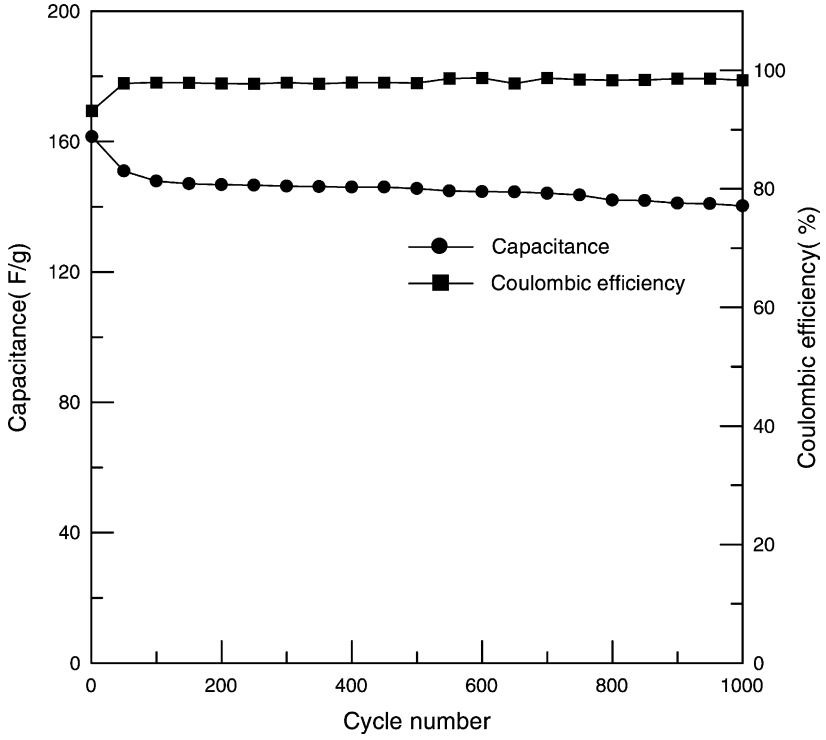

Fig. 10. Variation of capacitance and coulombic efficiency with cycle number for the PC electrode charged and discharged at 0.5 mA in 1 M H_2SO_4.

for both BC and PC electrodes are close to those evaluated from the simulation of the EIS data (Table 2).

The coulombic efficiencies (η) of the respective capacitors are also shown in Figs. 9 and 10, which are calculated according to

$$\eta = \left(\frac{t_D}{t_C}\right) \times 100 \quad (3)$$

where t_D and t_C are the expressions of discharge and charge times [18], respectively. The results reveal that the supercapacitors made by BC and PC electrodes have very stable coulombic efficiencies about 99% over 1000 cycles.

4. Conclusions

PANI was implanted on porous carbon by cyclic voltammetry to fabricate feasible composite electrodes for supercapacitors. The surface and composition information of the resulting electrodes were determined by SEM and XPS measurements. Electrochemical analyses, CV and ac impedance, show composite electrodes exhibiting higher capacitance than bare-carbon electrodes due to the addition of faradaic pseudocapacitance from PANI. From the simulation of EIS data with a proposed equivalent circuit, the pseudocapacitance was a strong function of the applied potentials. The practical performance and stability of the composite electrode were demonstrated by constant current charge–discharge cycling over 1000 cycles in 1 M H_2SO_4. A large value of 160 F/g in specific capacitance of the composite electrode was exhibited, and a capacitance increase of more than 60% was also achieved, in comparison with the bare-carbon electrode.

Acknowledgements

The authors are grateful to the National Science Council in Taiwan for its financial support through NSC 91-2214-E-006-028.

References

[1] D. Qu, J. Power Sources 109 (2002) 403.
[2] J. Gamby, P.L. Taberna, P. Simon, J.F. Fauvarque, M. Chesneau, J. Power Sources 101 (2001) 109.
[3] P.J. Mahon, G.L. Paul, S.M. Keshishian, A.M. Vassallo, J. Power Sources 91 (2000) 68.
[4] A. Celzard, F. Collas, J.F. Marêché, G. Furdin, I. Rey, J. Power Sources 108 (2002) 153.
[5] T.C. Weng, H. Teng, J. Electrochem. Soc. 148 (2001) A368.
[6] C.C. Hu, Y.H. Huang, K.H. Chang, J. Power Sources 108 (2002) 117.
[7] J. Hong, I.H. Yeo, W. Paik, J. Electrochem. Soc. 148 (2001) A156.
[8] K.S. Ryu, K.M. Kim, N.G. Park, Y.J. Park, S.H. Chang, J. Power Sources 103 (2002) 305.
[9] J.H. Park, O.O. Park, J. Power Sources 111 (2002) 185.
[10] J.H. Park, J.M. Ko, O.O. Park, D.W. Kim, J. Power Sources 105 (2002) 20.

[11] W.C. Chen, T.C. Wen, H. Teng, Electrochim. Acta 48 (2003) 641.
[12] H.S.O. Chan, S.C. Ng, W.S. Sim, K.L. Tan, B.T.G. Tan, Macromolecules 25 (1992) 6029.
[13] F. Fusalba, P. Gouerec, D. Villers, D. Belanger, J. Electrochem. Soc. 148 (2001) A1.
[14] C.C. Hu, C.H. Chu, J. Electroanal. Chem. 503 (2001) 105.
[15] Y.R. Nian, H. Teng, J. Electrochem. Soc. 149 (2002) A1008.
[16] M.A. Vorotyntsev, J.P. Badiali, G. Inzelt, J. Electroanal. Chem. 472 (1999) 7.
[17] R. Kotz, M. Carlen, Electrochim. Acta 45 (2000) 2483.
[18] T. Osaka, X. Liu, M. Nojima, T. Momma, J. Electrochem. Soc. 146 (1999) 1724.